BIOCHEMISTRY

© Copyright 2005 by the American Chemical Society Volume 44, Number 44 November 8, 2005

Articles

Role of the Unique Peptide Tail in Hyperthermostable *Aquifex aeolicus* Cochaperonin Protein 10[†]

Kathryn Luke,[‡] David Apiyo,[‡] and Pernilla Wittung-Stafshede*,[‡,§,||]

Department of Biochemistry and Cell Biology, Keck Center for Structural Computational Biology, and Department of Chemistry, Rice University, 6100 Main Street, Houston, Texas 77251

Received June 13, 2005; Revised Manuscript Received August 22, 2005

ABSTRACT: All known cochaperonin protein 10 (cpn10) molecules are heptamers of seven identical subunits noncovalently linked by β-strand interactions. Cpn10 from the deep-branching, hyperthermophilic bacterium *Aquifex aeolicus* (*Aa*cpn10) shows high homology with mesophilic and other thermophilic cpn10 sequences, except for a 25-residue C-terminal extension not found in any other cpn10. Prior to atomic structure information, we here address the role of the tail by biophysical means. A tail-lacking variant (*Aa*cpn10-*del25*) also adopts a heptameric structure in solution and exhibits nativelike substrate-refolding activity. Thermal and chemical perturbations of both *Aa*cpn10 and *Aa*cpn10-*del25*, probed by far-UV circular dichroism, demonstrate that both proteins have high thermodynamic stability. Heptamer−monomer dissociation midpoints were defined by isothermal titration calorimetry; at 25 °C, the values for *Aa*cpn10 and *Aa*cpn10-*del25* are within 2-fold of each other and close to reported midpoints for mesophilic cpn10 proteins. In contrast, the monomer stabilities for the *A. aeolicus* proteins are significantly higher than those of mesophilic homologues at 30 °C; thus, heptamer thermophily is a result of more stable monomers. Electron microscopy data reveals that *Aa*cpn10-*del25* heptamers are prone to stack on top of each other forming chainlike molecules; the electrostatic surface pattern of a structural model can explain this behavior. Taken together, the unique tail in *Aa*cpn10 is not required for heptamer structure, stability, or function; instead, it appears to be an ancient strategy to avoid cochaperonin aggregation at extreme temperatures.

Complexes resulting from noncovalent protein−protein recognition play a fundamental role in most biological functions. In addition to heterogeneous protein−protein complexes, many proteins are oligomeric due to the association of identical subunits (*1*). The function of quaternary structure, i.e., the arrangement of multiple subunits into an oligomer, may be to allow for cooperative effects or formation of novel active sites, provide additional stability, increase solubility, or decrease osmotic pressure (*2*). Reported folding pathways of oligomeric proteins (mostly dimers, trimers, and tetramers) reveal a variety of mechanisms (*3*−*7*). Some proteins display monomeric or oligomeric intermediates [e.g., *Escherichia coli* Trp repressor and the ATPase SecA (*8*, *9*)] whereas others fold in apparent two-state reactions in which folding and oligomerization are coupled [e.g., P22 Arc repressor (*10*, *11*)]. The heptameric

[†] Support for this project was provided by grants from NIH (GM059663) and the Robert A. Welch Foundation (C-1588). K.L. is supported by a fellowship from an NIH Biotechnology Research Training Grant.

* Corresponding author: e-mail, pernilla@rice.edu; fax, 1-713-348-5154; phone, 1-713-348-4076.

[‡] Department of Biochemistry and Cell Biology, Rice University.

[§] Keck Center for Structural Computational Biology, Rice University.

[||] Department of Chemistry, Rice University.

10.1021/bi051131l CCC: $30.25 © 2005 American Chemical Society
Published on Web 10/14/2005

cochaperonin protein 10 (cpn10) is an attractive model for studies of the interplay between polypeptide folding and protein−protein assembly. The primary function of the cpn10 heptamer is to assist cpn60 in folding of nonnative proteins. Upon binding to cpn60, cpn10 forms a cap covering the central cavity of cpn60, and folding of substrates (nonnative proteins) is achieved through cycles of ATP-dependent binding and dissociation (*12*−*15*). In addition to the established substrate-folding function, contemporary work shows that cpn10 proteins from different species have several other functions in, for example, pregnancy, cancer, immunogenic response, and protein-misfolding diseases (*16*−*21*).

Both structure and function of cpn10 appear conserved throughout nature (*12*−*15*). Crystal structures for *E. coli* cpn10 (GroES), *Mycobacterium tuberculosis* and *Mycobacterium leprae* cpn10, *Thermus thermophilus* cpn10, and bacteriophage T4 Gp31 proteins have been reported (*22*−*26*). Human mitochondrial cpn10 (*hm*cpn10) is 37% identical to GroES in terms of primary structure: X-ray and NMR data revealed that its overall fold is identical to that of GroES (*27*). In all known cases, each cpn10 subunit adopts an irregular β-barrel topology in the native heptamer. The dominant interaction between the subunits is an antiparallel pairing of the first β-strand in one subunit and the final β-strand in the other subunit (*22*). Biophysical work on *hm*cpn10 (*28*−*30*) and GroES (*31*−*33*) has shown that the isolated cpn10 monomers can be folded but that they have low stability (2.4−3 kJ/mol; 20 °C, pH 7). In both cases, more than 85% of the overall heptamer stability is governed by the interprotein interactions. Thermal unfolding reactions of GroES and *hm*cpn10 are apparent two-state equilibrium processes in which dissociation and unfolding are coupled (*30*, *31*). This is also the equilibrium mechanism observed upon GuHCl[1] additions to *hm*cpn10 (*30*) whereas GroES was reported to unfold via a partly folded monomeric intermediate in GuHCl (*32*).

Proteins from thermophilic organisms are often similar in sequence and structure to their mesophilic homologues, although they are much more resistant to thermal perturbation (*34*−*36*). The ability to remain active at high temperatures must thus come from a combination of subtle differences. Notably, hydrophobic interactions become less favorable, whereas charge−charge interactions get stronger, at higher temperatures (*37*, *38*). Several sources of thermostability have been proposed for different proteins; for example, stabilization by an increased number of ionic interactions, an increased extent of hydrophobic surface burial, more efficient residue packing, an increased number of prolines, and smaller surface loops (*35*, *36*, *39*−*42*). Less is known about the mechanisms that govern thermostability of *oligomeric* proteins, i.e., how stabilizing factors are divided between intra- and interprotein interactions. To address this issue, we have cloned cpn10 from the hyperthermostable organism *Aquifex aeolicus* (*Aa*cpn10) (*43*). *A. aeolicus* is a hyperthermophilic bacterium, capable of growing at 95 °C, for which the complete genome has been sequenced (*44*). *A. aeolicus* is among the most extreme thermophilic bacteria known and is thought to be one of the earliest bacteria to diverge from eubacteria. Despite the fact that this organism grows at bacteria's extreme thermal limit, only a few specific indications of its thermophily are apparent from the genome (*44*). Most characterized *A. aeolicus* proteins, as well as the amino acid sequences of assigned open reading frames, show high sequence similarity to their mesophilic counterparts. In this context, *Aa*cpn10 becomes an interesting exception. Each *Aa*cpn10 monomer exhibits high sequence homology with mesophilic and thermophilic cpn10 variants but has an extra C-terminal peptide extension of 25 amino acids not found in any other cpn10 molecule (*43*). The sequence of the tail (from N- to C-terminal: YSSLIGGEVRWQQRQLSTTRKQGQN) is not similar to any segment in any known protein according to BLAST searches.

Initial biophysical work has shown that *Aa*cpn10 adopts a heptameric structure in solution and that it functions as well as GroES and *hm*cpn10 in an in vitro GroEL-dependent substrate-refolding activity assay (*43*). Prior to atomic structure information, here we address the role of the unique tail by comparing the biophysical behavior of *Aa*cpn10 with a tail-lacking variant (*Aa*cpn10-*del25*). We find that *Aa*cpn10-*del25* adopts a heptameric structure, exhibits nativelike cochaperonin activity, and shows similar resistance to chemical and thermal perturbations as *Aa*cpn10. Upon dissecting the heptamer energetics into monomer and interface stabilities, respectively, it emerges that most of the increased stability of both *Aquifex* proteins, as compared to mesophilic cpn10 heptamers, stems from more stable monomers. The notable difference between *Aa*cpn10 and *Aa*cpn10-*del25* is that the latter is prone to aggregation; we explain this behavior by the electrostatic surface pattern of a structural model. We conclude that the in vivo role of the peptide tail in *Aa*cpn10 is to prevent heptamer aggregation and perhaps also block interactions with other *Aquifex* proteins.

MATERIALS AND METHODS

Preparation of Aacpn10 and Aacpn10-del25 and Simple Assays. E. coli expression and purification procedures for cpn10 from *A. aeolicus* (*Aa*cpn10) have been reported (*43*). The *A. aeolicus* deletion variant, lacking the last 25 residues at the C-terminus (abbreviated as *Aa*cpn10-*del25*), was created using the QuickChange site-directed mutagenesis kit (Stratagene). The truncation was confirmed by DNA sequencing. *Aa*cpn10-*del25* purification was similar to that of *Aa*cpn10 except that the heating step was performed at 55 °C and the buffer strength was changed from 50 to 25 mM Tris-HCl, pH 7.5. Protein concentrations were determined from $\epsilon_{280} = 11477\ M^{-1}\ cm^{-1}$ (*Aa*cpn10; one Trp in the C-terminal tail) and $\epsilon_{280} = 4460\ M^{-1}\ cm^{-1}$ (*Aa*cpn10-*del25*). All protein concentrations in this text are given per monomer. Gel filtration was performed on a calibrated 16/60 Superdex 75 column (Pharmacia) at 4 °C using an FPLC system. To avoid nonspecific binding of the cpn10 proteins to the gel matrix, 200 mM KCl was included in the buffer (*32*). For protein aggregation studies as a function of temperature, 50 μM *Aa*cpn10 and *Aa*cpn10-*del25* samples were incubated at temperatures ranging from 30 to 90 °C (in 10 °C steps) in a heat block for 15 min followed by cooling and then centrifugation to precipitate any aggregated species. The supernatant of each sample was loaded on an SDS−PAGE

[1] Abbreviations: CD, circular dichroism; ITC, isothermal titration calorimetry; EM, electron microscopy; AU, analytical ultracentrifugation; GuHCl, guanidine hydrochloride.

gel, and the subsequent protein bands were quantified using integrated density values (FluorChem 5500 multiimage light cabinet; Alpha Innotech).

GroEL-Dependent Substrate-Refolding Assay. The full procedure for the citrate synthase activity assay has been reported (*28*, *45*). In short, 30 μM pig heart citrate synthase (Boehringer Mannheim) was denatured in 6 M GuHCl (100 mM Tris-HCl, pH 8, 20 °C, 20 mM DTT) for 1 h. GuHCl was of highest grade from Sigma. While vortexing, denatured citrate synthase was diluted 100-fold into reaction mixtures containing 100 mM Tris-HCl, pH 8, 10 mM $MgCl_2$, 10 mM KCl, 4 μM GroEL, 2 μM cpn10, and 2 mM ATP. *E. coli* GroEL was purchased from Sigma. The mixtures were incubated for 2 h at 20 °C. Citrate synthase activity (catalyzing the condensation of oxaloacetate and acetyl-CoA to citrate and CoA) was measured by the decrease in absorption at 235 nm, which corresponds to acetyl-CoA disappearance. The reaction mixtures (40 μL) were added to 760 μL of 158 mM Tris-HCl, pH 7.6, 0.23 mM acetyl-CoA (Sigma), and 0.5 mM oxaloacetate (Sigma); the samples were mixed for 10 s and absorption at 235 nm and then monitored for 30 min. The percent recovery of citrate synthase activity was normalized to the activity of the native protein (i.e., not denatured).

Analytical Ultracentrifugation. Protein samples were subjected to sedimentation velocity analysis using a Beckman XL-A analytical ultracentrifuge. In one set of runs, the total monomer concentration was 60 and 170 μM for *Aa*cpn10 and *Aa*cpn10-*del25*, respectively, to achieve an absorption of ~0.7 at 280 nm, and in another set, the total monomer concentration was ~15 μM *Aa*cpn10-*del25* to achieve an absorption of ~0.7 at 230 nm. The temperature was kept at 20 °C. The rotor speed was 30000 rpm for all samples. The scans were analyzed by the software UltraScan (http://www.ultrascan.uthscsa.edu/) written by Borries Demeler (University of Texas Health Science Center, San Antonio, TX). All data were corrected for protein (using amino acid sequence) and buffer densities and solvent viscosity. To estimate molecular weights from the *S* values, shape factors for oblate and rod structures were used for the heptameric rings and the larger structures, respectively.

Thermally Induced Unfolding. Thermal unfolding was monitored by far-UV circular dichroism (CD) at 228 nm on Aviv 62A DS and Jasco J-810 instruments both equipped with digital thermal cells. In all CD measurements, the sample compartment was purged with nitrogen gas to avoid absorption by O_2. All reactions were reversible and occurred in single transitions (midpoint corresponding to T_m). Different equilibration times (5−10 min) at each temperature did not change the thermal profiles, and rescans of original samples gave identical results. Experiments were performed in 50 mM (*Aa*cpn10) and 25 mM (*Aa*cpn10-*del25*) Tris-HCl buffers (pH 7.5) and 1.25, 1.75, and 2.25 M GuHCl for protein concentrations (total monomer concentration) of 10, 50, and 100 μM. Linear extrapolations for each data set revealed the T_m in the absence of denaturant for that particular protein concentration. The scan rate was 60 °C/h, starting from 20 °C and going up to 90 °C, followed by slow cooling.

Chemically Induced Unfolding. Equilibrium unfolding of *Aa*cpn10-*del25* and *Aa*cpn10 at specific temperatures (30−90 °C) was monitored by far-UV CD and upon GuHCl additions. For most experiments, 50 μM total monomer concentration was used; at some temperatures (30 and 70 °C), titrations with 10, 50, and 100 μM protein concentrations were compared. In all cases, stock solutions of GuHCl were mixed with cpn10 solutions to give a fixed final protein concentration in each set of experiments. The equilibration time before measurements, at each experimental temperature, was 5−10 min (no effect on the unfolding behavior was observed for incubations times varying between 2 and 15 min). Unfolding of both *Aa*cpn10-*del25* and *Aa*cpn10 exhibited protein concentration dependence, and data analysis was performed using an apparent two-state reaction in which unfolding (subscript U) is coupled to dissociation (subscript D) (*30*):

$$F_{oligomer} \leftrightarrow 7U_{monomer} \quad (1)$$

The equilibrium constant for this reaction, K_{U+D}, and the free energy change, ΔG_{U+D}, for reaction 1 are defined as

$$K_{U+D} = [U_{monomer}]^7/[F_{oligomer}] \quad (2)$$

$$\Delta G_{U+D} = -RT \ln K_{U+D} \quad (3)$$

$[F_{oligomer}]$ is the concentration of folded oligomers (in molar) and $[U_{monomer}]$ is the concentration of unfolded monomers (in molar) at each GuHCl concentration. Standard concentrations of 1 M of all reactants are introduced; R is the gas constant and T is the absolute temperature. The use of 1 M protein concentration as the standard state is commonly used for concentration-dependent protein-unfolding reactions (*46*−*49*). The free energy change can be expressed as a function of denaturant (here, GuHCl) concentration:

$$\Delta G_{U+D} = \Delta G_{U+D}(H_2O) - m[\text{GuHCl}] \quad (4)$$

In this equation, m describes the sensitivity of the transition to GuHCl and is thought to reflect the extent of hydrophobic surface exposure upon unfolding (*50*). $\Delta G_{U+D}(H_2O)$ is the free energy of unfolding and dissociation in aqueous solution per mole of oligomer.

Since GuHCl is a salt in addition to being a denaturant, the free energies derived from these experiments may not be fully accurate (*51*−*54*). However, the nonionic denaturant urea could not be employed as a control since the two *A. aeolicus* proteins have high stability and urea is a weaker denaturant than GuHCl (*55*). Although unfolding of *Aa*cpn10-*del25* and *Aa*cpn10 begins at ~6 M urea (as detected by far-UV CD), unfolded state baselines are not established within the accessible concentration range of urea. Nonetheless, many stability studies on cpn10 proteins have been reported that use GuHCl as the denaturant (*28*, *30*, *32*, *56*, *57*).

Isothermal Titration Calorimetry (ITC). Measurements of heat changes linked to heptamer−monomer dissociation were made in a VP-ITC (MicroCal). The protein samples were dialyzed against 50 mM (*Aa*cpn10) and 25 mM (*Aa*cpn10-*del25*) Tris-HCl, pH 7.5. All samples were filtered through 0.22 μm sterile filter membrane (Millipore) and degassed (ThermoVac, MicroCal) before being loaded into the ITC syringe. Injection schedules that were found to cover appropriate protein concentration ranges in the cell (1.4 mL

volume) were 3 μL additions of 2−7 μM protein spaced between 5 min intervals. For both temperatures (25 and 50 °C) studied, at least two independent experiments were performed. The background heats from dilution of the proteins were estimated from the constant heats produced by the injections at very high protein concentrations (i.e., in the latter part of the titrations; here, the fraction of heptamer in the syringe and in the cell is roughly similar and close to 1). In each case, this value was subtracted out before the resulting isotherms were analyzed as described below. Attempts to obtain dissociation data at 70 °C failed due to high background signals and temperature-related noise.

ITC Data Analysis. The ITC data report on the individual heat change associated with each separate injection $q_{obs}(i)$. It was analyzed via an iterative nonlinear least-squares algorithm (*58*) to obtain K_D (i.e., the heptamer−monomer dissociation constant) and ΔH_D (i.e., the heptamer−monomer dissociation enthalpy; in per monomer units) using the relation between Y (fraction monomer) and $[M]_{tot}$ (total monomer concentration), which is a seventh-order polynomial:

$$Y^7 + (YK_D)/(7[M]_{tot}^6) - (K_D)/(7[M]_{tot}^6) = 0 \quad (5)$$

and the equation for the heat associated with each injection (*59*, *60*):

$$q_{obs}(i) = \Delta H_D[Y_i n(i) - Y_{i-1} n(i-1) - Y_{syr} n(\text{inj})] \quad (6)$$

In the latter equation, Y_i is the fraction of monomer in the cell after injection i, Y_{i-1} is the fraction of monomer in the cell after the previous, $i - 1$, injection, $n(i)$ is the number of moles of total monomer in the reaction cell after injection i ($=V[M]_{tot,i}$; V, reaction cell volume), and $n(i - 1)$ is the number of moles of total monomer in the reaction cell after injection $i - 1$ ($=V[M]_{tot,i-1}$). Y_{syr} is the fraction of monomers in the syringe (i.e., in the injected sample), and n(inj) is the number of moles of total monomers injected into the reaction cell at each injection ($=v[M]_{tot,syr}$; v is injected volume).

Using an assigned value of K_D and the protein concentration in the syringe ($[M]_{tot,syr}$), eq 5 was first solved to obtain the fraction of monomer in the syringe (Y_{syr}). Next, accounting for the protein concentration in the syringe, the cell volume, and the injection volume, the total concentration of protein in the cell after each injection i was calculated ($[M]_{tot,i}$). Then, the fraction of monomers (Y_i) in the cell was calculated after each injection i by solving eq 5. From the increment in monomer concentration in the cell after each injection, also accounting for the fraction of monomers coming directly from the syringe, the heat associated with each injection was calculated according to eq 6 and an assigned value of ΔH_D. The calculated heats were compared with the experimental ones, and the complete procedure was repeated until convergence was achieved and the experimental $q_{obs}(i)$ versus $[M]_{tot}$ data could be accurately reproduced (*58*). K_D is related to the Gibbs free energy of dissociation via $\Delta G_D = -RT \ln K_D$, and ΔS_D is calculated from $\Delta G_D = \Delta H_D - T\Delta S_D$.

Electron Microscopy. The proteins were diluted to various total monomer concentrations in 50 mM (*Aa*cpn10) and 25 mM (*Aa*cpn10-*del25*) Tris-HCl buffer, pH 7.5, adsorbed to a freshly prepared thin carbon foil, washed in distilled water, and stained with 0.75% uranyl formate. Transmission electron microscopy was performed using a JEOL2010 electron microscope. The micrographs were recorded on a CCD detector at 50000× nominal magnification.

Computer Modeling. The *Aa*cpn10 monomer was modeled through a homology search using SWISS-MODEL (*61*, *62*). The 122-residue sequence was searched against proteins with homologous sequences in the Protein Data Bank. The resulting structure for the *Aa*cpn10 monomer was modeled on the basis of the crystal structure of *T. thermophilus* cpn10. The C-terminal 25 residues were ignored in the search, and thus the output model is one of *Aa*cpn10-*del25*. *T. thermophilus* and *A. aeolicus* cpn10 sequences are 57% identical if the 25-residue tail is ignored. An overlay of the C_αs of the two structures (the *Aa*cpn10-*del25* model and the *T. thermophilus* cpn10 crystal structure) shows a nearly perfect fit (RMS deviation of 0.3 Å) with the exception of a four-residue region (residues 21−24 in *T. thermophilus* which correspond to residues 17−20 in *A. aeolicus*). Next, seven copies of the *Aa*cpn10-*del25* monomer were created and named as different chains. The *T. thermophilus* cpn10 heptamer (1WE3) was used as template on which the seven monomers of *Aa*cpn10-*del25* were merged in Swiss-PDB Viewer. The created data file was then submitted to SWISS-MODEL for modeling of the *Aa*cpn10-*del25* heptameric structure. The electrostatic surface potential of the *Aa*cpn10-*del25* heptamer structure was calculated by solving the Poisson−Boltzmann function using Delphi in the software GRASP (*63*, *64*). The ionic strength was set to 0.1 M, and all histidines were protonated.

RESULTS

Oligomeric State and Cochaperonin Function. Initial biophysical characterization of *Aa*cpn10 revealed that this hyperthermostable molecule retains many hallmark characteristics of mesophilic cpn10 molecules, including the heptameric structure (*43*). However, the polypeptide of each *Aa*cpn10 monomer is 122 residues long, with the last 25 amino acids not found in any other cpn10 molecule. To elucidate the role of this unique tail, we prepared a deletion variant that lacks the last 25 C-terminal residues (*Aa*cpn10-*del25*).

Both *Aa*cpn10 and *Aa*cpn10-*del25* samples elute as heptamers in gel filtration experiments (not shown). Gluteraldehyde cross-linking results of *Aa*cpn10 and *Aa*cpn10-*del25* are similar: a set of bands corresponding to monomers, dimers, trimers, tetramers, pentamers, hexamers, and heptamers are observed at 20 °C. This behavior was previously assigned to the lysine side chains not being fully available for cross-linking in the heptamer at this temperature (*43*). Notably, cross-linking of *Aa*cpn10 and *Aa*cpn10-*del25* becomes dominated by heptamers when the temperature is increased (not shown). This suggests that the heptameric structures become more flexible at higher temperatures, which makes the lysines more available for the cross-linker. Electron microscopy (EM) images at 4 °C demonstrate the presence of ring-shaped molecules, in support of nativelike heptamers, for both *Aa*cpn10 and *Aa*cpn10-*del25* samples (Figure 1A,B).

The quaternary structures of *Aa*cpn10 and *Aa*cpn10-*del25* were also assessed by analytical ultracentrifugation (AU).

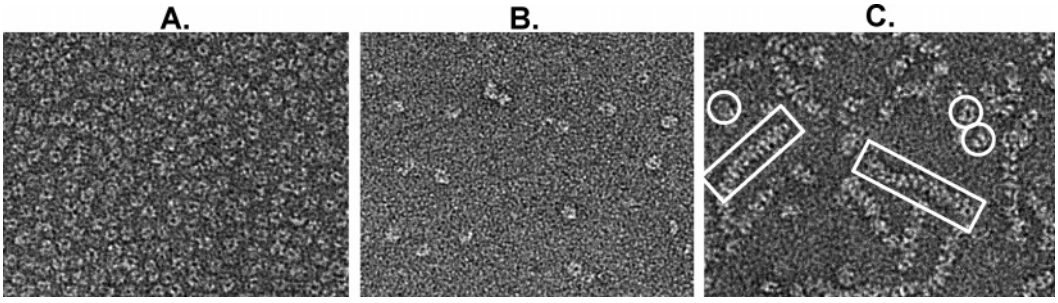

FIGURE 1: Transmission electron microscopy images of *Aa*cpn10-*del25* (panel A, ~20 μM monomer concentration), *Aa*cpn10-*del25* (panel B, ~5 μM monomer concentration), and *Aa*cpn10-*del25* (panel C, ~30 μM monomer concentration) at 4 °C. The micrographs were recorded at 50000× nominal magnification. In (C), a few representative single rings are circled and aggregates of stacked rings boxed in white.

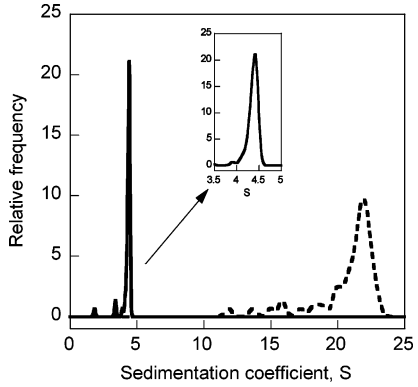

FIGURE 2: Sedimentation−velocity data showing relative frequency versus *S*-values (data analyzed using UltraScan software) for *Aa*cpn10 (solid line) and *Aa*cpn10-*del25* (dashed line) samples at 60 and 170 μM monomer concentration, respectively. Both samples appear as rather pure components with sedimentation coefficients of about 4.4 and 22 S, respectively. Inset: Enlargement of the 4−5 S region. Analysis of samples with lower *Aa*cpn10-*del25* concentrations (below 50 μM) results in a mixture of two species with 4.1 and ~19 S, respectively (not shown).

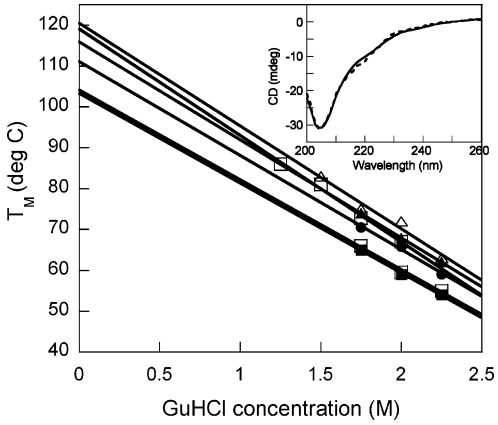

FIGURE 3: Thermal midpoints (T_m), determined from CD-monitored unfolding curves, for *Aa*cpn10 (open symbols) and *Aa*cpn10-*del25* (filled symbols) as a function of GuHCl concentration for 10 (squares), 50 (circles, and squares at 1.25 and 1.5 M), and 100 (triangles) μM total monomer concentrations (pH 7). Linear extrapolation gives T_m in the absence of denaturant in each case (Table 1). Inset: Far-UV CD signals of *Aa*cpn10 (solid line) and *Aa*cpn10-*del25* (dashed line), 20 °C.

According to sedimentation velocity measurements, *Aa*cpn10 has a sedimentation coefficient near 4.4 S (Figure 2). This value is slightly larger than previously published *S* values for GroES (*33*) and corresponds to an estimated molecular mass of ~90 kDa if a shape factor for an oblate ellipsoid (1.45) is used. Noting that the true structure is ring-shaped, this estimate is in good agreement with the actual 95 kDa molecular mass of *Aa*cpn10. Sedimentation velocity experiments with *Aa*cpn10-*del25* (at >100 μM protein) reveal larger molecules with a sedimentation coefficient of 22 S (Figure 2). However, AU experiments at lower protein concentrations (i.e., 20 μM protein; samples with <20 μM protein did not give enough signal) display a distribution of two sedimentation coefficients, one of ~4.1 S and one of ~19 S (data not shown). An *S* of 4.1 corresponds to a molecular mass of ~75 kDa (using an oblate ellipsoid shape factor) which is the actual molecular mass of heptameric *Aa*cpn10-*del25*. This result supports that *Aa*cpn10-*del25* can form heptamers but emphasizes that it has a tendency to aggregate at higher protein concentrations (further discussed below).

To test the similarity of *Aa*cpn10-*del25* to *Aa*cpn10 in terms of function, and as another method to confirm heptameric structures, an in vitro activity assay was performed (*30*, *45*). GroEL-dependent refolding of citrate synthase was measured in the presence of the two *A. aeolicus* cpn10 proteins. The two proteins gave identical results in terms of promoting citrate synthase refolding: both *Aa*cpn10-*del25* and *Aa*cpn10 promoted 26 ± 1% refolding of citrate synthase at our conditions (see Materials and Methods). At the exact same conditions, GroES has been reported to promote 28% refolding of citrate synthase (*45*). In addition, an earlier study revealed that *Aa*cpn10 and *hm*cpn10 promote citrate synthase refolding with similar efficiencies (*43*). As a negative control, a mutant *hm*cpn10 that does not assemble into heptamers (*28*) resulted in less than 3% refolding of citrate synthase in this assay.

*Stability toward Thermal Perturbations. Hm*cpn10 and GroES, in accord with being mesophilic, have thermal midpoints around 70 °C at pH 7 (*30*, *31*). The reversible, equilibrium transitions are protein concentration dependent since unfolding and disassembly are coupled in the thermal reactions. In Figure 3, we show thermal midpoints (probed by far-UV CD) for *Aa*cpn10 and *Aa*cpn10-*del25*, at different protein concentrations, as a function of GuHCl concentrations to lower the transitions to below 100 °C. The inset in Figure 3 shows CD spectra of *Aa*cpn10 and *Aa*cpn10-*del25* at 20 °C; both proteins have the characteristic cpn10-like CD signal as reported for GroES (*31*, *32*). Extrapolation of the midpoints, for each protein concentration, yields the thermal midpoint in the absence of denaturant in each case (Table 1). Like *hm*cpn10 and GroES (*30*, *31*), the thermal processes for *Aa*cpn10 and *Aa*cpn10-*del25* are reversible and protein concentration dependent, suggesting a coupled unfolding/

Table 1: Thermal Midpoints (T_m) in the Absence of Denaturant (Figure 3) for *Aa*cpn10 and *Aa*cpn10-*del25* as a Function of Protein Concentration (Total Monomer Concentration), pH 7.5

variant	10 μM	50 μM	100 μM
*Aa*cpn10	106 (±2)	119 (±2)	121 (±2)
*Aa*cpn10-*del25*	103 (±2)	111 (±2)	116 (±2)
*hm*cpn10[a]	71	73	
GroES[b]	70	74	75

[a] From ref *30*. [b] From ref *31*.

dissociation reaction: the more protein present, the higher the midpoint. Notably, there is only a nominal difference in the thermal behavior of *Aa*cpn10 and *Aa*cpn10-*del25*: the wild-type protein is slightly more heat stable.

Stability toward Chemical Perturbations. Since *Aa*cpn10 and *Aa*cpn10-*del25* are stable in a wide temperature range, we investigated their stability toward chemical perturbation at several temperatures. In Figure 4A, we show the GuHCl concentrations at the midpoints of the equilibrium unfolding transitions (probed by far-UV CD) as a function of temperature. In all cases, the transitions have sigmoidal shapes and are at least 90% reversible. The unfolding processes were investigated in detail at two selected temperatures: 30 and 70 °C (Figure 4B; Table 2). At both temperatures, protein concentration dependence in the transition midpoints is observed. This is similar to the thermal behavior and to the behavior of *hm*cpn10 upon GuHCl additions at room temperature (*30*). Therefore, the data were fitted to a seven-to-one reaction mechanism (*30*), and free energies for the coupled unfolding/dissociation reactions were estimated (Table 2). Interestingly, although the midpoints shift to lower GuHCl concentrations at the higher temperature, as expected, the free energy associated with the reaction remains roughly the same.

Heptamer−Monomer Dissociation Reactions. Self-association processes leading to homooligomeric complexes have usually not been studied by isothermal titration calorimetry (ITC), except for a few dimeric cases (*59*, *60*, *65*). We recently demonstrated that complete thermodynamic descriptions (i.e., K_D, ΔG, ΔH, and ΔS) for self-associating systems with high molecularity can be obtained by ITC dilution experiments (*58*). With a protein concentration in the syringe above the midpoint for dissociation, ensuring oligomers, injections into a buffer-filled cell can result in sufficient dilution so that oligomer dissociation is triggered; upon proper analysis (*58*), the corresponding heat changes for such titrations can be used to derive thermodynamic parameters (see Materials and Methods). In Figure 5, we show the heat changes (in calories per mole of injectant) as a function of total monomer concentration in the cell for ITC dilution experiments with *Aa*cpn10 (A) and *Aa*cpn10-*del25* (B) at 25 °C. It is immediately clear that, in both cases, heptamer dissociation corresponds to negative enthalpy which, therefore, means that association is an endothermic process. Similar experiments were repeated at 50 °C and analyzed as described in Materials and Methods; the resulting thermodynamic parameters are reported in Table 3.

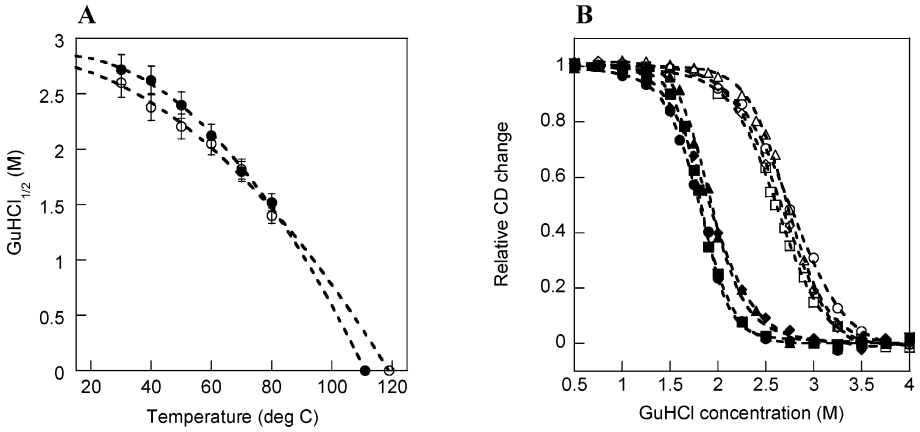

FIGURE 4: (A) GuHCl-induced transition midpoints, monitored by far-UV CD, for 50 μM *Aa*cpn10 (open symbols) and *Aa*cpn10-*del25* (filled symbols) as a function of temperature. The T_m values, defined in Figure 3, for 50 μM protein (corresponding to the transition midpoints at 0 M GuHCl) are also marked. (B) GuHCl-induced unfolding of *Aa*cpn10 (30 °C, open squares/triangles; 70 °C, filled squares/triangles) and *Aa*cpn10-*del25* (30 °C, open circles/diamonds; 70 °C, filled circles/diamonds) at two different total protein concentrations (50 μM, squares and circles; 100 μM, triangles and diamonds). Each transition was fit to an apparent two-state folded heptamer-to-unfolded monomer transition (see Table 2).

Table 2: GuHCl Concentrations at Transition Midpoints ([GuHCl]$_{1/2}$) and Corresponding Free Energies for Heptamer-to-Monomer Reactions [$\Delta G_{U+D}(H_2O)$, Values Given per Heptamer] for *Aa*cpn10 and *Aa*cpn10-*del25* Unfolding/Dissociation Processes Induced by GuHCl as a Function of Protein Concentration (Total Monomer Concentration) and Solution Temperature (T) at pH 7.5[a]

		10 μM		50 μM		100 μM		
protein variant	T (°C)	[GuHCl]$_{1/2}$ (M)	$\Delta G_{U+D}(H_2O)$ (kJ/mol)	[GuHCl]$_{1/2}$ (M)	$\Delta G_{U+D}(H_2O)$ (kJ/mol)	[GuHCl]$_{1/2}$ (M)	$\Delta G_{U+D}(H_2O)$ (kJ/mol)	average (kJ/mol)
*Aa*cpn10	30	1.3 (±0.1)	267 (±5)	2.6 (±0.1)	266 (±5)	2.7 (±0.1)	265 (±5)	~266
*Aa*cpn10	70	1.1 (±0.1)	266 (±5)	1.8 (±0.1)	261 (±5)	2.0 (±0.1)	262 (±5)	~263
*Aa*cpn10-*del25*	30	2.5 (±0.1)	284 (±5)	2.7 (±0.1)	279 (±5)	2.8 (±0.1)	281 (±5)	~281
*Aa*cpn10-*del25*	70	1.5 (±0.1)	281 (±5)	1.8 (±0.1)	284 (±5)	1.9 (±0.1)	285 (±5)	~283
*hm*cpn10[b]	20			1.5	216 (±10)	2.8	218 (±10)	~216

[a] 50 and 100 μM data shown in Figure 4B. [b] From ref *30*.

Table 3: Thermodynamic Parameters for the Heptamer−Monomer Equilibria for *Aa*cpn10-*del25* and *Aa*cpn10 Calculated from the ITC Dilution Experiments As Described in Materials and Methods[a]

protein	T (°C)	midpoint (μM)	ΔG_A (kJ/mol)	ΔH_A (kJ/mol)	ΔS_A [J/(mol·K)]
*Aa*cpn10-*del25*	25	0.51 (±0.03)	−32 (±0.5)	+186 (±4)	+732 (±15)
*Aa*cpn10-*del25*	50	0.55 (±0.03)	−34 (±0.5)	+96 (±4)	+402 (±15)
*Aa*cpn10	25	0.27 (±0.03)	−33 (±0.5)	+36 (±4)	+232 (±10)
*Aa*cpn10	50	0.43 (±0.03)	−35 (±0.5)	+67 (±4)	+316 (±10)
*hm*cpn10[d]	20	3.0[b]	−27.8		
GroES[e]	20	0.7[c]	−31		

[a] For comparison, available heptamer−monomer midpoints for GroES and *hm*Cpn10 are also shown. All values correspond to assembly (indicated by subscript A) at the indicated temperature and are given per mole of monomer. [b] From dilution experiments measuring fluorescence changes. [c] From analytical ultracentrifugation experiments. [d] From ref *30*. [e] From ref *75*.

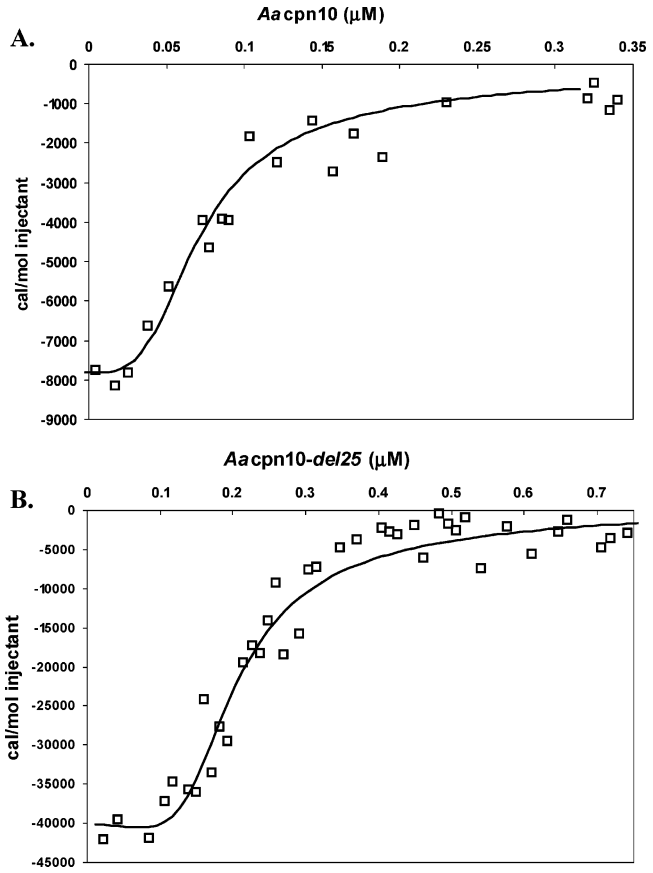

FIGURE 5: ITC dilution data (heat changes, ΔH_i, in calories per mole of injectant versus total monomer concentration in the cell with fits overlaid) for (A) *Aa*cpn10 and (B) *Aa*cpn10-*del25* at 25 °C. Thermodynamic parameters were derived as described in Materials and Methods (see Table 3).

Aggregation Behavior. For *Aa*cpn10-*del25* samples of high protein concentration, protein aggregates are observed in the EM images in addition to single rings (Figure 1C). These larger structures are consistent with side views of "stacks" of rings, forming chainlike molecules. The length of the chains depended on the protein concentration; the higher the *Aa*cpn10-*del25* concentration, the longer the chains, and less nonassociated rings were observed. In accord, the AU experiments (Figure 2) with high *Aa*cpn10-*del25* concentrations demonstrate the presence of a population of large molecules with an *S* value of 22. Using a shape factor for a rod, this corresponds to molecular masses in the range of 500−600 kDa.

Protein incubation studies as a function of temperature show that *Aa*cpn10-*del25* is more prone than *Aa*cpn10 to aggregation in a temperature-dependent fashion. For example,

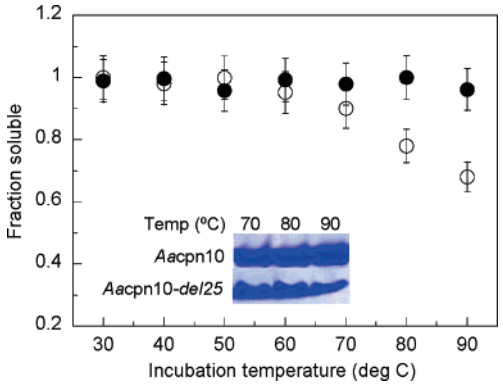

FIGURE 6: Fraction of soluble *Aa*cpn10 (filled circles) and *Aa*cpn10-*del25* (open circles) after 15 min incubation at temperatures between 30 and 90 °C. After incubation, the samples were centrifuged, and the supernatant of each sample was loaded on an SDS−PAGE gel, followed by quantification. Inset: SDS−PAGE bands for the 70, 80, and 90 °C samples.

incubation at 80 and 90 °C leads to 20% and 30% reductions, respectively, in soluble *Aa*cpn10-*del25* after 15 min. In contrast, at the same conditions, less than 3% of *Aa*cpn10 samples are lost to aggregation (Figure 6).

Structural Modeling of the Aquifex Heptamer. Homology modeling using *Aa*cpn10-*del25*'s primary structure predicts a fold for the *Aa*cpn10-*del25* monomer that is indistinguishable from that of the *T. thermophilus* cpn10 monomer (Figure 7A). The *T. thermophilus* cpn10 sequence is 57% identical to that of *Aa*cpn10-*del25*. The C-terminal tail cannot be modeled since it exhibits no homology to anything in the PDB. On the basis of the monomer model, a heptamer structure was assembled (Figure 7B). The electrostatic surface potential for the *Aa*cpn10-*del25* heptamer is much more negative than that of GroES and *T. thermophilus* cpn10 (Figure 7C). Notably, the mobile loop β-hairpins of *Aa*cpn10-*del25* have a higher density of charged residues as compared to GroES and *hm*cpn10. We imagine that *Aa*cpn10-*del25* rings interact via intermolecular salt bridges between heptamers stacking on top of each other.

DISCUSSION

Cpn10 proteins are ring-shaped heptamers that appear conserved throughout nature. β-Strand pairing between the N-terminus of one subunit and the C-terminus of another is the major source of interactions at the subunit−subunit interfaces. There are 86 full-length sequences of cpn10 molecules from different species in SwissPROT; only cpn10 from *A. aeolicus*, which is a hyperthermostable ancestral bacterium, contains a C-terminal peptide extension. Here we

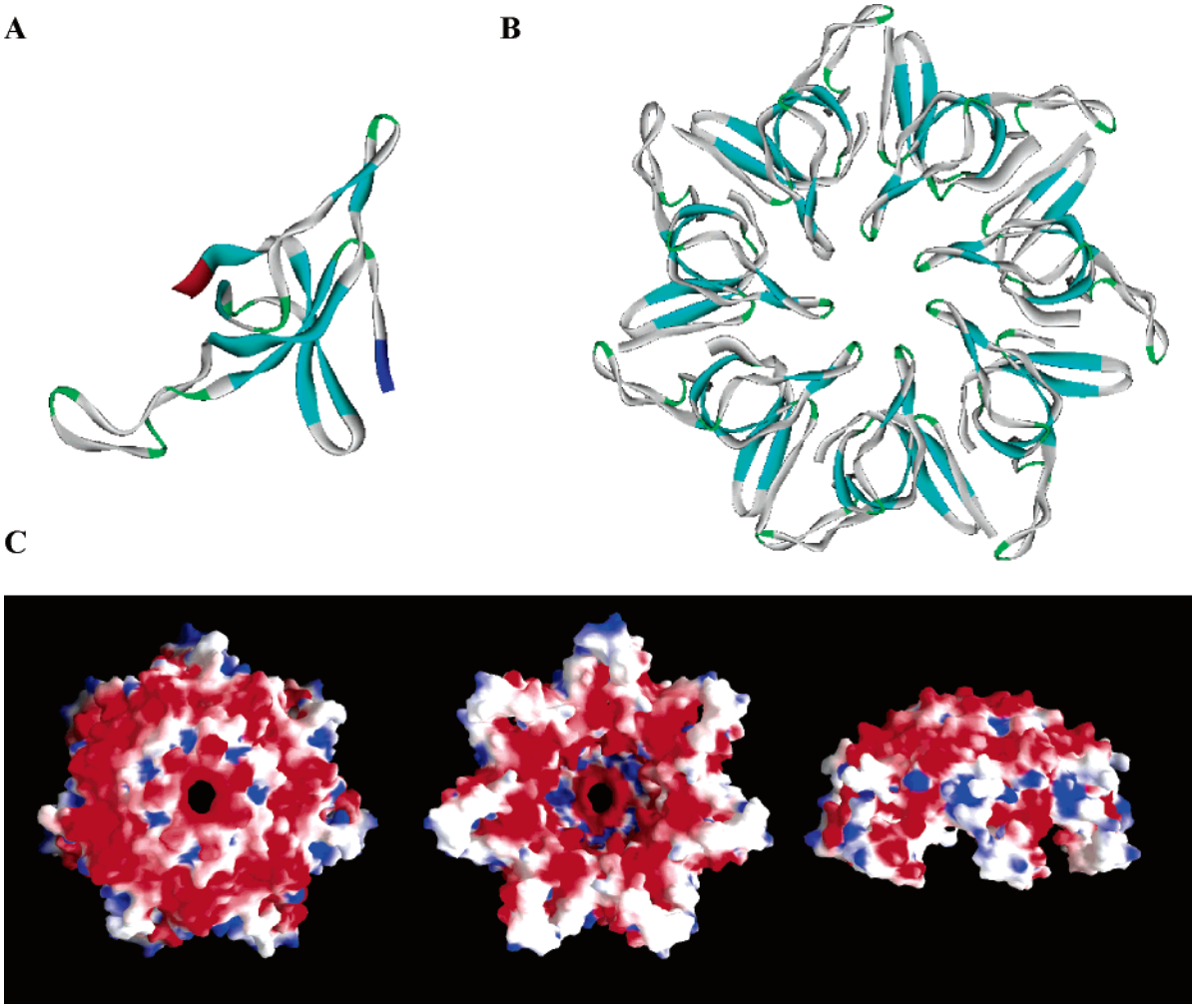

FIGURE 7: (A) Ribbon diagram of the *Aa*cpn10-*del25* monomer model. The N-terminus is shown in blue and the C-terminus in red. (B) Ribbon diagram of the structural model of the *Aa*cpn10-*del25* heptamer. In both (A) and (B), light blue corresponds to β-strand, gray to coil, and green to turn secondary structure elements. (C) Electrostatic surface potential (scale ranges from −5 to 5 kT) of the *Aa*cpn10-*del25* heptamer calculated by GRASP (red, negative; blue, positive; white, neutral potential). From left to right: top view, bottom view, and side view of the *Aa*cpn10-*del25* heptamer.

have assessed the role of the unique peptide tail in *Aa*cpn10 by comparing the biophysical behavior of *Aa*cpn10 with a tail-lacking variant (*Aa*cpn10-*del25*). We find that *Aa*cpn10-*del25* adopts a heptameric structure (by gel filtration, cross-linking, EM, and AU experiments), exhibits nativelike refolding activity, and shows roughly similar resistance to chemical and thermal perturbations as *Aa*cpn10 (Figures 3 and 4; Tables 1 and 2). In addition, the heptamer−monomer dissociation midpoints are within 2-fold of each other for *Aa*cpn10-*del25* and *Aa*cpn10 and, moreover, are similar to midpoints for other cpn10 proteins (Figure 5 and Table 3; the corresponding free energies are within ±15% of each other). This suggests that the the C-terminal tail is not important for cochaperonin function, heptamer stability, or heptamer assembly. By comparing our findings on the *A. aeolicus* proteins to reported data on mesophilic cpn10 proteins, we can obtain insight into sources of thermophily in this oligomeric protein system. First, it is clear from Figure 4A that the two *A. aeolicus* oligomers exhibit modest temperature dependence in their stability toward GuHCl perturbation. That the free energy profile for a thermophilic protein would be a flattened version of that for the mesophilic protein has been proposed as one model to explain higher stability of thermostable proteins (*35*, *36*, *39*−*42*). Small temperature dependence can be achieved via low heat capacity changes associated with the unfolding reactions. This will be the case if the thermostable protein's unfolded state has less entropy than that of the corresponding mesophilic protein (*66*, *67*); in support of this mechanism, *Aa*cpn10 has many more prolines than GroES.

The GuHCl-induced transitions for the *A. aeolicus* proteins report on coupled unfolding/dissociation processes, and thus the free energies estimated for the processes (ΔG_{U+D}; see Table 2) are truly the sum of the free energy for heptamer dissociation into seven monomers (ΔG_{Diss}) and the free energies for unfolding of the seven monomers ($7\Delta G_U$) as follows:

$$\Delta G_{U+D} = 7\Delta G_U + \Delta G_{Diss}$$

Since the free energies associated with heptamer−monomer dissociation have been determined independently by ITC, we can use the above thermodynamic cycle to estimate the unfolding free energies of the monomers (ΔG_U). Using ΔG_{U+D} at 30 °C (Table 2) and ΔG_{Diss} at 25 °C (Table 3; note that there is only minor temperature dependence in

ΔG_{Diss}), we derive monomer stabilities of 5.1±1.0 and 8.0±1.0 kJ/mol for *Aa*cpn10 and *Aa*cpn10-*del25*, respectively. These values can be compared to reported monomer stabilities (20 °C, pH 7) of 2.4 and 3.0 kJ/mol for GroES and *hm*cpn10, respectively (*30*, *32*). Thus, monomer stability is increased by 100−200% in the *A. aeolicus* proteins. Taken together with the comparable monomer−monomer affinities, it emerges that most of the increased stability of the *A. aeolicus* proteins, as compared to mesophilic cpn10 heptamers, stems from more stable monomers. Comparison of the amino acid sequences of *Aa*cpn10, *hm*cpn10, and GroES demonstrates that the *A. aeolicus* cpn10 proteins harbor many of the hallmark features, mentioned in the introduction, that are associated with increased stability. For example, the ratio of charged to polar residues, (E + K)/(Q + H), is generally higher for thermostable proteins; in accord, GroES has such a ratio of 18 whereas *Aa*cpn10-*del25* has a ratio of 26. Moreover, GroES has only 2% prolines and 16% negatively charged residues whereas *Aa*cpn10-*del25* has 6% prolines and 21% negatively charged residues. To somewhat of a surprise, the *Aa*cpn10-*del25* monomers are more stable than the *Aa*cpn10 monomers at 30 °C. The reason for this is elusive although speculations include (i) that the C-terminal extension makes more favorable interactions in the unfolded, than in the folded, monomeric state (the peptide extension is highly charged and long-range ionic interactions may form in the unfolded state) or (ii) that the presence of the C-terminal tail causes some disruption of the structure in the core of the folded monomer. Both explanations are in agreement with the C-terminal extension being in a flexible, solvent-exposed state in the folded *Aa*cpn10 monomers (see further arguments below).

The ITC dilution experiments demonstrate that the assembly processes of *Aa*cpn10 and *Aa*cpn10-*del25* are accompanied by unfavorable (i.e., endothermic) enthalpy and favorable (i.e., positive) entropy (Table 3). This can be explained by the release of ordered water molecules from the monomer surfaces that form the interfaces (*68*). This reaction is enthalpically unfavorable since it involves the breakage of hydrogen and ionic bonds. The positive entropy associated with assembly follows the classical hydrophobic effect, which is an entropy-driven process. Partitioning of a nonpolar molecule from water to a nonpolar phase is accompanied by an increase in the entropy of the system (*69*). Since the *Aa*cpn10 interfaces are mostly hydrophobic, there may be a significant number of ordered waters released upon assembly. The positive entropy and enthalpy values associated with assembly are smaller in magnitude for *Aa*cpn10 than for *Aa*cpn10-*del25* at both temperatures (Table 3). This may be explained by *Aa*cpn10 assembly involving also folding of the C-terminal peptide. Such a reaction is enthalpically favorable, but entropically unfavorable, and will thus lower the positive magnitudes of ΔH_A and ΔS_A. This observation supports that the C-terminal tail adopts an ordered structure and makes tertiary interactions in the *Aa*cpn10 heptamer but not in the monomers. The crystal structure of the *Aa*cpn10 heptamer may directly establish the conformation of the tail and what tertiary interactions it is making (work in progress). Inspection of the data in Table 3 also reveals that the unfavorable enthalpy and favorable entropy changes upon assembly are decreased at the higher temperature for *Aa*cpn10-*del25*. This is likely an effect of the increased water mobility at higher temperatures; at these conditions, less ordered water molecules are bound to the monomers, resulting in less water released upon assembly.

The only significant difference discovered in this study between *Aa*cpn10 and *Aa*cpn10-*del25* is that the latter is prone to stacking (i.e., ordered aggregation) as demonstrated by EM and AU experiments as well as high-temperature incubations. The fact that *Aa*cpn10-*del25* oligomers aggregate although this behavior has never been observed with *hm*cpn10 or GroES may be due to differences in overall electrostatic surface potential and amino acid composition. *Aa*cpn10-*del25* has a much more negative overall surface potential, and a higher density of positive and negative charges in the mobile loops, than GroES and *hm*cpn10 (Figure 7). We propose that head-to-tail ring−ring stacking via intermolecular charge−charge interactions results in the observed chainlike aggregates (Figure 1C). Theoretical work has shown that salt bridges often stabilize protein−protein interactions (*70*). Moreover, it was noted that protein−protein interfaces can have like charge pairs; this may shift the pK_a of the ionizable groups so that one or both become neutral or the pairs may form triads with opposite charges or, if the charges are solvent accessible, counterions may bind to balance the like charges (*70*). The involvement of counterions offers an explanation for how the stacking is possible in the context of the highly negative top and bottom surfaces of the *Aa*cpn10-*del25* rings.

A similar type of ring−ring stacking interactions as we observe herein has been reported for a heptameric minichromosome maintenance (MCM) protein from *Methanobacterium thermoautotrophicum* (*71*). Cpn10 from *M. tuberculosis* was shown by crystallography and light scattering experiments to form a complex of two heptamers that were associated face to face through hydrophobic mobile loop interactions (*72*). However, *Aa*cpn10-*del25* stacking cannot be based on the same type of interactions as in *M. tuberculosis* cpn10 given that then only dimers would be observed. Because stacking is not observed with *Aa*cpn10, the hydrophilic tail with its many positive charges may sterically shield interactions between the heptamers (it also increases the p*I* from 4.7 to 5.1). In analogy, it has been reported that fusions of charged peptide extensions to the C-termini of large proteins can rescue these proteins from aggregation and precipitation during bacterial overexpression (*73*). We propose that the in vivo role of the unique tail in *Aa*cpn10 is to prevent heptamer−heptamer aggregation and unwanted interactions with other proteins.

We note that there exists one other report of an *A. aeolicus* protein that has a peptide insertion not found in homologous proteins from other species. The editing domain of leucyl-tRNA synthetase (LeuRS) from *A. aeolicus* has a 20-residue insertion not found in any other bacterial LeuRSs (*74*). The authors speculate that this peptide motif disappeared during the evolution of LeuRSs due to the acquisition of new tRNA-binding domains that helped to stabilize the editing activity. In the case of cpn10, we propose that the extra peptide tail in the ancient hyperthermophilic *A. aeolicus* variant was lost during evolution due to (i) point mutations altering the surface charge patterns as well as (ii) decreased growing temperatures of mesophilic organisms.

ACKNOWLEDGMENT

We thank Jesse Guidry (Louisiana State University) for preparing *Aa*cpn10-*del25*, Susan Cates (Rice University) for assistance with analytical ultracentrifugation, Zanhua Xie (Rice University) for conducting electron microscopy experiments, and Mingzhi Chen (Baylor College of Medicine) for calculating the electrostatic surface potential.

REFERENCES

1. Traut, T. W. (1994) Dissociation of enzyme oligomers: a mechanism for allosteric regulation, *Crit. Rev. Biochem. Mol. Biol. 29*, 125−163.
2. Darnall, D. W., and Klotz, I. M. (1975) Subunit constitution of proteins: a table, *Arch. Biochem. Biophys. 166*, 651−682.
3. Bodenreider, C., Kellershohn, N., Goldberg, M. E., and Mejean, A. (2002) Kinetic analysis of R67 dihydrofolate reductase folding: from the unfolded monomer to the native tetramer, *Biochemistry 41*, 14988−14999.
4. Ziegler, M. M., Goldberg, M. E., Chaffotte, A. F., and Baldwin, T. O. (1993) Refolding of luciferase subunits from urea and assembly of the active heterodimer. Evidence for folding intermediates that precede and follow the dimerization step on the pathway to the active form of the enzyme, *J. Biol. Chem. 268*, 10760−10765.
5. Mann, C. J., Shao, X., and Matthews, C. R. (1995) Characterization of the slow folding reactions of trp aporepressor from *Escherichia coli* by mutational analysis of prolines and catalysis by a peptidyl-prolyl isomerase, *Biochemistry 34*, 14573−14580.
6. Waldburger, C. D., Jonsson, T., and Sauer, R. T. (1996) Barriers to protein folding: formation of buried polar interactions is a slow step in acquisition of structure, *Proc. Natl. Acad. Sci. U.S.A. 93*, 2629−2634.
7. Nichtl, A., Buchner, J., Jaenicke, R., Rudolph, R., and Scheibel, T. (1998) Folding and association of beta-Galactosidase, *J. Mol. Biol. 282*, 1083−1091.
8. Gloss, L. M., and Matthews, C. R. (1998) Mechanism of folding of the dimeric core domain of *Escherichia coli* trp repressor: a nearly diffusion-limited reaction leads to the formation of an on-pathway dimeric intermediate, *Biochemistry 37*, 15990−15999.
9. Doyle, S. M., Braswell, E. H., and Teschke, C. M. (2000) SecA folds via a dimeric intermediate, *Biochemistry 39*, 11667−11676.
10. Milla, M. E., and Sauer, R. T. (1994) P22 Arc repressor: folding kinetics of a single-domain, dimeric protein, *Biochemistry 33*, 1125−1133.
11. Srivastava, A. K., and Sauer, R. T. (2000) Evidence for partial secondary structure formation in the transition state for arc repressor refolding and dimerization, *Biochemistry 39*, 8308−8314.
12. Martin, J., Geromanos, S., Tempst, P., and Hartl, F. U. (1993) Identification of nucleotide-binding regions in the chaperonin proteins GroEL and GroES, *Nature 366*, 279−282.
13. Todd, M. J., Boudkin, O., Freire, E., and Lorimer, G. H. (1995) GroES and the chaperonin-assisted protein folding cycle: GroES has no affinity for nucleotides, *FEBS Lett. 359*, 123−125.
14. Burston, S. G., Weissman, J. S., Farr, G. W., Fenton, W. A., and Horwich, A. L. (1996) Release of both native and non-native proteins from a cis-only GroEL ternary complex, *Nature 383*, 96−99.
15. Shtilerman, M., Lorimer, G. H., and Englander, S. W. (1999) Chaperonin function: folding by forced unfolding, *Science 284*, 822−825.
16. Athanasas-Platsis, S., Somodevilla-Torres, M. J., Morton, H., and Cavanagh, A. C. (2004) Investigation of the immunocompetent cells that bind early pregnancy factor and preliminary studies of the early pregnancy factor target molecule, *Immunol. Cell Biol. 82*, 361−369.
17. Cappello, F., Bellafiore, M., David, S., Anzalone, R., and Zummo, G. (2003) Ten kilodalton heat shock protein (HSP10) is overexpressed during carcinogenesis of large bowel and uterine exocervix, *Cancer Lett. 196*, 35−41.
18. Slavotinek, A. M., and Biesecker, L. G. (2001) Unfolding the role of chaperones and chaperonins in human disease, *Trends Genet. 17*, 528−535.
19. Coates, A. R. M. (1996) *The Chaperonins*, Academic Press, London.
20. Cavanagh, A. C., and Morton, H. (1994) The purification of early-pregnancy factor to homogeneity from human platelets and identification as chaperonin 10, *Eur. J. Biochem. 222*, 551−560.
21. Cavanagh, A. C. (1996) Identification of early pregnancy factor as chaperonin 10: implications for understanding its role, *Rev. Reprod. 1*, 28−32.
22. Hunt, J. F., Weaver, A. J., Landry, S. J., Gierasch, L., and Deisenhofer, J. (1996) The crystal structure of the GroES co-chaperonin at 2.8 Å resolution, *Nature 379*, 37−45.
23. Mande, S. C., Mehra, V., Bloom, B. R., and Hol, W. G. (1996) Structure of the heat shock protein chaperonin-10 of *Mycobacterium leprae*, *Science 271*, 203−207.
24. Roberts, M. M., Coker, A. R., Fossati, G., Mascagni, P., Coates, A. R., and Wood, S. P. (1999) Crystallization, X-ray diffraction and preliminary structure analysis of *Mycobacterium tuberculosis* chaperonin 10, *Acta Crystallogr., Sect. D: Biol. Crystallogr. 55*, 910−914.
25. Hunt, J. F., van der Vies, S. M., Henry, L., and Deisenhofer, J. (1997) Structural adaptations in the specialized bacteriophage T4 co-chaperonin Gp31 expand the size of the Anfinsen cage, *Cell 90*, 361−371.
26. Numoto, N., Kita, A., and Miki, K. (2005) Crystal structure of the co-chaperonin Cpn10 from *Thermus thermophilus* HB8, *Proteins 58*, 498−500.
27. Landry, S. J., Steede, N. K., and Maskos, K. (1997) Temperature dependence of backbone dynamics in loops of human mitochondrial heat shock protein 10, *Biochemistry 36*, 10975−10986.
28. Guidry, J. J., Shewmaker, F., Maskos, K., Landry, S., and Wittung-Stafshede, P. (2003) Probing the interface in a human co-chaperonin heptamer: Residues disrupting oligomeric unfolded state identified, *BMC Biochem. 4*, 14.
29. Guidry, J. J., and Wittung-Stafshede, P. (2002) Low stability for monomeric human chaperonin protein 10: interprotein interactions contribute majority of oligomer stability, *Arch. Biochem. Biophys. 405*, 280−282.
30. Guidry, J. J., Moczygemba, C. K., Steede, N. K., Landry, S. J., and Wittung-Stafshede, P. (2000) Reversible denaturation of oligomeric human chaperonin 10: denatured state depends on chemical denaturant, *Protein Sci. 9*, 2109−2117.
31. Boudker, O., Todd, M. J., and Freire, E. (1997) The structural stability of the co-chaperonin GroES, *J. Mol. Biol. 272*, 770−779.
32. Higurashi, T., Nosaka, K., Mizobata, T., Nagai, J., and Kawata, Y. (1999) Unfolding and refolding of *Escherichia coli* chaperonin GroES is expressed by a three-state model, *J. Mol. Biol. 291*, 703−713.
33. Seale, J. W., Gorovits, B. M., Ybarra, J., and Horowitz, P. M. (1996) Reversible oligomerization and denaturation of the chaperonin GroES, *Biochemistry 35*, 4079−4083.
34. Jaenicke, R., and Bohm, G. (1998) The stability of proteins in extreme environments, *Curr. Opin. Struct. Biol. 8*, 738−748.
35. Szilagyi, A., and Zavodszky, P. (2000) Structural differences between mesophilic, moderately thermophilic and extremely thermophilic protein subunits: results of a comprehensive survey, *Struct. Folding Des. 8*, 493−504.
36. Rees, D. C., and Adams, M. W. (1995) Hyperthermophiles: taking the heat and loving it, *Structure 3*, 251−254.
37. Privalov, P. (1997) Thermodynamics of protein Folding, *J. Chem. Thermodyn. 29*, 447−474.
38. Privalov, P. L., and Makhatadze, G. I. (1993) Contribution of hydration to protein folding thermodynamics. II. The entropy and Gibbs energy of hydration, *J. Mol. Biol. 232*, 660−679.
39. Beadle, B. M., Baase, W. A., Wilson, D. B., Gilkes, N. R., and Shoichet, B. K. (1999) Comparing the thermodynamic stabilities of a related thermophilic and mesophilic enzyme, *Biochemistry 38*, 2570−2576.
40. Hollien, J., and Marqusee, S. (1999) A thermodynamic comparison of mesophilic and thermophilic ribonucleases H, *Biochemistry 38*, 3831−3836.
41. McCrary, B. S., Edmondson, S. P., and Shriver, J. W. (1996) Hyperthermophile protein folding thermodynamics: differential scanning calorimetry and chemical denaturation of Sac7d, *J. Mol. Biol. 264*, 784−805.
42. Vogt, G., Woell, S., and Argos, P. (1997) Protein thermal stability, hydrogen bonds, and ion pairs, *J. Mol. Biol. 269*, 631−643.
43. Guidry, J., and Wittung-Stafshede, P. (2004) First characterization of co-chaperonin protein 10 from hyper-thermophilic *Aquifex aeolicus*, *Biochem. Biophys. Res. Commun. 317*, 176−180.

44. Deckert, G., Warren, P. V., Gaasterland, T., Young, W. G., Lenox, A. L., Graham, D. E., Overbeek, R., Snead, M. A., Keller, M., Aujay, M., Huber, R., Feldman, R. A., Short, J. M., Olsen, G. J., and Swanson, R. V. (1998) The complete genome of the hyperthermophilic bacterium *Aquifex aeolicus*, *Nature 392*, 353−358.
45. Buchner, J., Schmidt, M., Fuchs, M., Jaenicke, R., Rudolph, R., Schmid, F. X., and Kiefhaber, T. (1991) GroE facilitates refolding of citrate synthase by suppressing aggregation, *Biochemistry 30*, 1586−1591.
46. Barry, J. K., and Matthews, K. S. (1999) Thermodynamic analysis of unfolding and dissociation in lactose repressor protein, *Biochemistry 38*, 6520−6528.
47. Bowie, J. U., and Sauer, R. T. (1989) Equilibrium dissociation and unfolding of the Arc repressor dimer, *Biochemistry 28*, 7139−7143.
48. Dams, T., and Jaenicke, R. (1999) Stability and folding of dihydrofolate reductase from the hyperthermophilic bacterium *Thermotoga maritima*, *Biochemistry 38*, 9169−9178.
49. Panse, V. G., Swaminathan, C. P., Aloor, J. J., Surolia, A., and Varadarajan, R. (2000) Unfolding thermodynamics of the tetrameric chaperone, SecB, *Biochemistry 39*, 2362−2369.
50. Schellman, J. A. (1987) Selective binding and solvent denaturation, *Biopolymers 26*, 549−559.
51. Smith, J. S., and Scholtz, J. M. (1996) Guanidine hydrochloride unfolding of peptide helices: separation of denaturant and salt effects, *Biochemistry 35*, 7292−7297.
52. Santoro, M. M., and Bolen, D. W. (1988) Unfolding free energy changes determined by the linear extrapolation method. 1. Unfolding of phenylmethanesulfonyl alpha-chymotrypsin using different denaturants, *Biochemistry 27*, 8063−8068.
53. Santoro, M. M., and Bolen, D. W. (1992) A test of the linear extrapolation of unfolding free energy changes over an extended denaturant concentration range, *Biochemistry 31*, 4901−4907.
54. Yao, M., and Bolen, D. W. (1995) How valid are denaturant-induced unfolding free energy measurements? Level of conformance to common assumptions over an extended range of ribonuclease A stability, *Biochemistry 34*, 3771−3781.
55. Makhatadze, G. I., and Privalov, P. L. (1992) Protein interactions with urea and guanidinium chloride. A calorimetric study, *J. Mol. Biol. 226*, 491−505.
56. Brown, C., Liao, J., and Wittung-Stafshede, P. (2005) Interface mutation in heptameric co-chaperonin protein 10 destabilizes subunits but not interfaces, *Arch. Biochem. Biophys. 439*, 175−183.
57. Sakane, I., Ikeda, M., Matsumoto, C., Higurashi, T., Inoue, K., Hongo, K., Mizobata, T., and Kawata, Y. (2004) Structural stability of oligomeric chaperonin 10: the role of two beta-strands at the N and C termini in structural stabilization, *J. Mol. Biol. 344*, 1123−1133.
58. Luke, K., Apiyo, D., and Wittung-Stafshede, P. (2005) Dissecting homo-heptamer thermodynamics by isothermal titration calorimetry: Entropy-driven assembly of co-chaperonin protein 10, *Biophys. J.* (in press).
59. Velazquez-Campoy, A., Leavitt, S. A., and Freire, E. (2004) Characterization of protein−protein interactions by isothermal titration calorimetry, *Methods Mol. Biol. 261*, 35−54.
60. Burrows, S. D., Doyle, M. L., Murphy, K. P., Franklin, S. G., White, J. R., Brooks, I., McNulty, D. E., Scott, M. O., Knutson, J. R., Porter, D., and et al. (1994) Determination of the monomer−dimer equilibrium of interleukin-8 reveals it is a monomer at physiological concentrations, *Biochemistry 33*, 12741−12475.
61. Guex, N., and Peitsch, M. C. (1997) SWISS-MODEL and the Swiss-PdbViewer: an environment for comparative protein modeling, *Electrophoresis 18*, 2714−2723.
62. Schwede, T., Kopp, J., Guex, N., and Peitsch, M. C. (2003) SWISS-MODEL: An automated protein homology-modeling server, *Nucleic Acids Res. 31*, 3381−3385.
63. Honig, B., and Nicholls, A. (1995) Classical electrostatics in biology and chemistry, *Science 268*, 1144−1149.
64. Nicholls, A., Sharp, K. A., and Honig, B. (1991) Protein folding and association: insights from the interfacial and thermodynamic properties of hydrocarbons, *Proteins 11*, 281−296.
65. Lovatt, M., Cooper, A., and Camilleri, P. (1996) Energetics of cyclodextrin-induced dissociation of insulin, *Eur. Biophys. J. 24*, 354−357.
66. Kumar, S., Tsai, C. J., and Nussinov, R. (2001) Thermodynamic differences among homologous thermophilic and mesophilic proteins, *Biochemistry 40*, 14152−14165.
67. Robertson, A. D., and Murphy, K. P. (1997) Protein structure and the energetics of protein stability, *Chem. Rev. 97*, 1251−1267.
68. Abraham, T., Lewis, R. N., Hodges, R. S., and McElhaney, R. N. (2005) Isothermal titration calorimetry studies of the binding of a rationally designed analogue of the antimicrobial peptide gramicidin S to phospholipid bilayer membranes, *Biochemistry 44*, 2103−2112.
69. Tanford, C. (1978) The hydrophobic effect and the organization of living matter, *Science 200*, 1012−1018.
70. Xu, D., Lin, S., and Nussinov, R. (1997) Protein binding versus protein folding: The role of hydrophilic bridges in protein associations, *J. Mol. Biol. 265*, 68−84.
71. Yu, X., VanLoock, M. S., Poplawski, A., Kelman, Z., Xiang, T., Tye, B. K., and Egelman, E. H. (2002) The *Methanobacterium thermoautotrophicum* MCM protein can form heptameric rings, *EMBO Rep. 3*, 792−797.
72. Roberts, M. M., Coker, A. R., Fossati, G., Mascagni, P., Coates, A. R., and Wood, S. P. (2003) *Mycobacterium tuberculosis* chaperonin 10 heptamers self-associate through their biologically active loops, *J. Bacteriol. 185*, 4172−4185.
73. Zhang, Y. B., Howitt, J., McCorkle, S., Lawrence, P., Springer, K., and Freimuth, P. (2004) Protein aggregation during overexpression limited by peptide extensions with large net negative charge, *Protein Expression Purif. 36*, 207−216.
74. Zhao, M. W., Zhu, B., Hao, R., Xu, M. G., Eriani, G., and Wang, E. D. (2005) Leucyl-tRNA synthetase from the ancestral bacterium *Aquifex aeolicus* contains relics of synthetase evolution, *EMBO J. 24*, 1430−1439.
75. Zondlo, J., Fisher, K. E., Lin, Z., Ducote, K. R., and Eisenstein, E. (1995) Monomer-heptamer equilibrium of the *Escherichia coli* chaperonin GroES, *Biochemistry 34*, 10334−10339.

BI051131L